# $\alpha$-Glucosidase and $\alpha$-Amylase Inhibitors from *Arcytophyllum thymifolium*

Luigi Milella,[†] Stella Milazzo,[‡] Marinella De Leo,[‡] Mariela Beatriz Vera Saltos,[⊥] Immacolata Faraone,[†] Tiziano Tuccinardi,[‡,§] Margherita Lapillo,[‡] Nunziatina De Tommasi,*[,‖] and Alessandra Braca[‡,§]

[†]Dipartimento di Scienze, Università degli Studi della Basilicata, Viale dell'Ateneo Lucano 10, 85100 Potenza, Italy

[‡]Dipartimento di Farmacia, Università di Pisa, via Bonanno 6 and 33, 56126 Pisa, Italy

[§]Centro Interdipartimentale di Ricerca "Nutraceutica e Alimentazione per la Salute", Università di Pisa, via del Borghetto 80, 56124 Pisa, Italy

[⊥]Departamento de Ciencias de la Vida, Universidad de las Fuerzas Armadas, ESPE, Av. General Rumiñahui s/n, Sangolqui, Ecuador

[‖]Dipartimento di Farmacia, Università degli Studi di Salerno, via Giovanni Paolo II 132, 84084 Fisciano (SA), Italy

**ABSTRACT:** Three new coumarins (**1**-**3**), a prenylated flavanone (**4**), and two iridoids (**5** and **6**), together with seventeen known secondary metabolites, were isolated from the aerial parts of *Arcytophyllum thymifolium*. The structures of the new compounds were elucidated on the basis of their spectroscopic data. The potential hypoglycemic properties of the new and known compounds were evaluated by measuring their $\alpha$-amylase and $\alpha$-glucosidase inhibitory effects. The iridoid asperulosidic acid (**15**) and the flavonoid rhamnetin (**13**) showed the highest activities vs $\alpha$-amylase ($IC_{50}$ = 69.4 ± 3.1 and 73.9 ± 5.9 μM respectively). In turn, the new eriodictyol derivative **4** exhibited the most potent effect as an $\alpha$-glucosidase inhibitor, with an $IC_{50}$ value of 28.1 ± 2.6 μM, and was more active than acarbose, used as a positive control. Modeling studies were also performed to suggest the interaction mode of compound **4** in the $\alpha$-glucosidase enzyme active site.

The genus *Arcytophyllum* (Rubiaceae) comprises 15 species that are distributed mainly in the tropical mountains of Central and South America. The majority of these species are present in Ecuador where they grow between 2500 and 4000 a.s.l. in the typical Andean grass paramo and paramo forest ecosystems.[1,2] Infusions and/or decoctions of the aerial parts of *Arcytophyllum* sp., locally known as "canllye", are used in Andean traditional medicine for the treatment of colic and indigestion.[3] The genus is almost completely uninvestigated from both the chemical and biological points of view, with only one previous study reported in the literature that showed the presence of iridoids, flavonoids and triterpenoids from *A. nitidum*.[4]

In an investigation of bioactive metabolites from plants belonging to the Ecuadorian flora,[5,6] the aerial parts of *A. thymifolium* (Ruiz & Pav.) Standl., a shrub up to 45 cm with small opposite leaves and small white flowers,[1] was selected as the subject of this study. Chemical investigation led to the identification of six new compounds, including three coumarins (**1**-**3**), a prenylated flavanone (**4**), and two iridoids (**5** and **6**), together with seventeen known secondary metabolites constituted by five coumarins (**7**-**11**), three flavonols (**12**-**14**), seven iridoids (**15**-**21**), and two quinic acid derivatives (**22**-**23**). Recently, the inhibition of the $\alpha$-amylase and $\alpha$-glucosidase enzymes has attracted attention as an important strategy in the treatment of diabetes and/or obese patients, since inhibitors of these enzymes can retard the uptake of dietary carbohydrates and reduce prostprandial hyperglycemia. Several investigations were reported in the literature on plant constituents such as coumarins,[7] flavonoids,[8-10] iridoids[11,12] and quinic acid derivatives[13] as potential leads for the development of inhibitors. A number of lead compounds have been obtained from natural sources, of which some are of clinical importance.[14-16] Thus, as a part of a project searching for new $\alpha$-amylase and $\alpha$-glucosidase inhibitors useful for the treatment of type 2 diabetes mellitus, all compounds isolated from *A. thymifolium* were screened biologically and molecular modeling studies were performed on the lead compound **4**.

## RESULTS AND DISCUSSION

The aerial parts of *A. thymifolium* were extracted with solvents of increasing polarity to afford *n*-hexane, chloroform, and methanol residues. The methanol extract was partitioned between *n*-butanol and $H_2O$ to give a *n*-BuOH residue. The $CHCl_3$ and *n*-BuOH extracts were subjected to different chromatographic procedures to afford six new (**1**-**6**) and 17 known compounds (**7**-**23**).

Compound **1** was isolated as a pale yellow powder. Its molecular formula was established as $C_{15}H_{14}O_6$ by means of HRESIMS (*m/z* 291.0803 $[M + H]^+$, 313.0657 $[M + Na]^+$) and the $^{13}C$- NMR spectrum. The UV spectrum ($\lambda_{max}$ 304 and 253 nm) indicated the presence of a coumarin nucleus.[17] Its 600 MHz NMR spectrum (Table 1) showed characteristic coumarin doublets at δ 6.39 and 8.06 (*J* = 9.4 Hz) for H-3 and H-4, and one singlet signal at δ 7.06 for H-5, which indicated the presence of a penta-substituted aromatic ring. Another singlet signal at δ 4.03 (3H, s) was assigned to an aromatic methoxy group. The other $^1H$ NMR chemical shifts suggested an angular 6-methoxy-pyranocoumarin skeleton. Three further singlets at δ 7.02 (1H, s), 3.78 (2H, s) and 1.62 (3H, s), attributable to an olefinic proton, a hydroxymethylene and a methyl group, respectively, were also observed. The connectivity of each proton to the respective carbon was confirmed by the HSQC spectrum, while the assignments of the $^{13}C$ NMR data (Table 1) were accomplished by a HMBC experiment. The basic skeleton of todannin was recognized in **1** by comparison with data reported previously in the literature.[18] In particular, the HMBC spectrum showed that the signal at *δ* 7.02 (H-4') correlated with those at *δ* 120.9 (C-8) and 164.5 (C-3'); Me-6' (*δ* 1.62) and $H_2$-5' (*δ* 3.78) showed correlations with C-2' (*δ* 73.0) and C-3' (*δ* 164.5); H-5 (*δ* 7.06) correlated with C-6 (*δ* 144.5), C-7 (*δ* 147.0), and H-4 (*δ* 8.06) correlated with C-2 (*δ* 162.3), C-5 (*δ* 100.0), and C-8a (*δ* 143.9). The cross peak between *δ* 4.03 ($OCH_3$) and 144.5 ppm (C-6) confirmed the presence of a methoxy group at C-6. The relative configuration of **1** was determined through a NOESY experiment: key correlations were observed between *δ* 1.62 (Me-6') and 4.03 (OMe) and 7.06 (H-5), indicating that the methyl

group is on the same side of the methoxy group. On the basis of the above evidence, the structure of **1** was determined as 5'-hydroxy-3'-dehydro-toddanin, a new natural coumarin.

The molecular formula of compound **2** ($C_{14}H_{12}O_6$) was determined by its HRESIMS ($[M + H]^+$ ion at *m/z* 277.0698) and by its $^{13}C$ NMR data. The negative-ion ESIMS showed a major peak at *m/z* 275 $[M - H]^-$ and two fragments at *m/z* 245 $[M - H - 30]^-$ and 201 $[M - H - 30 - 44]^-$. Comparison of the NMR spectroscopic data of **2** with those of **1** (Table 1) showed that these compounds differ only in the absence of the methoxy group at C-6 in **2**. Hence compound **2** was assigned as 6-demethyl-5'-hydroxy-3'-dehydro-toddanin.

The HRESIMS of compound **3** exhibited a pseudomolecular ion at *m/z* 293.1046 $[M - H]^-$, consistent with the molecular formula $C_{15}H_{18}O_6$. In the HRESIMS/MS three major fragments at *m/z* 278.0853 (due to the loss of 15 mass units), 205.0618 (due to the loss of 88 mass units), and 190.0384 (due to the loss of 15 and 88 mass units) were observed. The UV spectrum suggested **3** as possessing a similar coumarin core to **1**. The $^1H$ NMR spectrum of **3** (Table 1) exhibited, in addition to protons of a coumarin skeleton, signals for a 2,3-dihydroxy-isopentyl group at $\delta$ 1.30 (6H, s, H-4' and H-5'), 3.04 (1H, br d, $J$ = 13.0 Hz, H-1'b), 3.20 (1H, dd, $J$ = 13.0, 10.5 Hz, H-1'a), and 3.73 (1H, m, H-2'). The $^{13}C$ NMR spectrum of **3** (Table 1) revealed the presence of 15 carbon resonances, which were sorted into two methyl, one methoxy, one methylene, four methine, and seven quaternary carbons. The chemical shift assignments of the carbon atoms were established from the HSQC and HMBC spectra. Key HMBC correlations between H-4—C-2, H-4—C-5; H-5—C-6, H-5—C-8a; H-1'—C-8, H-1'—C-8a, H-1'—C-2'; Me-4'/Me-5'—C-1', Me-4'/Me-5'—C-2'; OMe—C-6, were observed and supported the locations of the methoxy group at C-6 and the 2,3-dihydroxy-isopentyl group at C-8. The configuration of the 2'-hydroxy group was assigned tentatively as *R* through the Snatzke method.[19] The expected negative Cotton effects for the *R* stereoisomer at 245 and 308 nm were weakly observed. From all these data, the new compound **3** was characterized as (2'*R*)-7-hydroxy-8-(2',3'-dihydroxyisopentyl)-6-methoxycoumarin.

The molecular formula of compound **4** was determined as $C_{20}H_{20}O_6$ by HRESIMS (*m/z* 379.1156 $[M + Na]^+$) and $^{13}C$ NMR data analysis. The UV spectrum of **4** showed two absorption maxima at 330 and 288 nm, indicating a flavanone skeleton. Compound **4** was deduced to be a prenyloxy eriodictyol derivative[20] on the basis of its $^1H$ NMR spectrum (Table 2). Thus, a 5,7-disubstituted pattern for ring A (two doublets at $\delta$ 6.04 and 6.06) and a 3',4'-disubstitution for ring B (ABX system signals at $\delta$ 6.81 and 6.82 overlapped signals; 6.95 (d, $J$ = 2.0 Hz), two methyl singlets at $\delta$ 1.76 and 1.80 and one methine proton at $\delta$ 5.44 (t, $J$ = 6.5 Hz) were evident. The twenty $^{13}C$ NMR resonances (Table 2) were attributed to an eriodictyol moiety and a prenyloxy group. Assignments of the $^1H$ NMR chemical shifts of **4** were accomplished by 1D-TOCSY, DQF-COSY, HSQC, and HMBC experiments. Key correlation peaks were observed in the HMBC experiment between $\delta$ 6.95 (H-2') and 80.8 (C-2), 147.0 (C-4'), and 119.3 (C-6'), $\delta$ 6.04 (H-6) and 168.4 (C-7) and 104.2 (C-10), $\delta$ 4.58 (H-1") and 168.4 (C-7), 139.7 (C-3"), $\delta$ 3.13 and 2.74 (H-3a and H-3b) and 80.8 (C-2), 197.9 (C-4), 132.0 (C-1'), $\delta$ 1.80 (H-4") and 120.0 (C-2") and 18.3 (C-5"). The relative configuration at C-2 was assigned as *S* on the basis of a negative Cotton effect at 270 nm in the CD spectrum of **4**.[21] In the light of these data, the structure of **4** was elucidated as (2*S*)-7-prenyloxy-eriodictyol, a new natural flavanone.

The molecular formula of compound **5** was assigned as $C_{24}H_{28}O_{13}$ by HRESIMS (*m/z* 523.1459 $[M - H]^-$) and $^{13}C$ NMR data analysis, equating for 11 degrees of unsaturation. In the ESIMS/MS spectrum, a peak at *m/z* 361 $[M - H - 162]^-$, due to the loss of one hexose unit, was observed. Its UV spectrum showed an absorption maximum at 252 nm for an aromatic ring conjugated with a carboxylic function. The $^1H$ NMR (Table 2) showed the presence of an iridoid glucoside, with a double bond at $\delta$ 6.09 (1H, d, $J$ = 2.0 Hz), a hydroxylated methine group at $\delta$ 4.90 (1H, overlapped signal), a hydroxylated methylene group at $\delta$ 5.00 and 5.25 (each 1H, br d, $J$ = 15.0 Hz), and a methoxy group bonded to a carboxylic acid group at $\delta$ 3.78 (3H, s). The $^{13}C$ NMR spectra (Table 2) of **5** showed 24 signals, of which ten were assigned to an iridoid aglycone moiety, while the remaining 14 signals corresponded to a hexose sugar unit, a *p*-hydroxybenzoyl functionality and a

methoxy group. The aglycone moiety of **5** was identified as deacetyl asperulosidic acid methyl ester.[22] The *p*-hydroxybenzoyl group was located at C-10 on the basis of the chemical shifts of $H_2$-10 at $\delta$ 5.00 and 5.25, typically shifted downfield by esterification. On the basis of these data, **5** was characterized as 10-*O*-*p*-hydroxybenzoyl deacetyl asperulosidic acid methyl ester.

Compound **6** was assigned the molecular formula, $C_{23}H_{24}O_{12}$, by HRESIMS (*m/z* 491.4320 $[M - H]^-$) and from its NMR spectra. Its ESIMS/MS spectrum showed a fragment at *m/z* 329 $[M - H - 162]^-$ and 191 $[M - H - 162 - 138]^-$ due to the sequential loss of one hexose unit and one *p*-hydroxybenzoyl group. The $^1H$ and $^{13}C$ NMR spectra (Table 2) revealed resonances typical of a cyclopentanopyran-type iridoid glucoside showing two olefinic protons at $\delta$ 5.81 (1H, br s) and 7.32 (1H, s), an oxymethine proton at $\delta$ 6.05 (1H, d, $J$ = 8.0 Hz), and a hydroxymethylene group at $\delta$ 4.70 (1H, d, $J$ = 15.0 Hz) and 4.82 (1H, d, $J$ = 15.0 Hz). Moreover, signals for a hexose sugar unit and a *p*-hydroxybenzoyl group were evident. On NMR spectroscopic data comparison, it was apparent that **6** possesses a C-6/C-11 lactone ring as in asperuloside (**20**). The $CH_2$ signals at $\delta$ 4.70 and 4.82 in the $^1H$ NMR spectrum and $\delta$ 62.8 in the $^{13}C$ NMR spectrum suggested that the C-10 hydroxy group is the position of esterification. Therefore, the structure of **6** was concluded to be 10-*O*-*p*-hydroxybenzoyl deacetyl asperuloside.

Compound **7** was identified as cneorumcoumarin B by comparison of its $^1H$ NMR and other spectroscopic values with those reported in the literature. It was previously isolated only in *Cneorum pulverulentum* Vent. (Rutaceae) in 1975[23] and its full NMR assignments have not been reported in the literature. Therefore, a 2D NMR study of **7** was performed and its complete $^1H$ and $^{13}C$ NMR chemical shifts are reported in Table 1.

Compounds **8**-**23** were characterized as hedyotiscone A (**8**),[24] toddanin (**9**),[18] hedyotiscone B (**10**),[24] fraxetin (**11**),[25] quercetin 3-*O*-*β*-D-galactopyranoside (**12**),[26] rhamnetin (**13**),[27] kaempferol 3-*O*-*β*-D-glucopyranosyl-(1→2)-*β*-D-galactopyranoside (**14**),[28] asperulosidic acid (**15**),[22] deacetyl asperulosidic acid methyl ester (**16**),[22] asperulosidic acid methyl ester (**17**),[29] scandoside (**18**),[30,31] deacetyl asperuloside (**19**),[22] asperuloside (**20**),[22] 10-*O*-*p*-hydroxybenzoyl scandoside methyl ester

(**21**),[22] neochlorogenic acid methyl ester (**22**),[32] and chlorogenic acid (**23**)[33] by spectroscopic data analysis and comparison with literature values.

All isolates were screened for their in vitro inhibitory activities against the *α*-amylase and *α*-glucosidase enzymes. The results are expressed as $IC_{50}$ (μM) and were compared with acarbose, used as a positive control (Figure 1).[5] Several compounds (**1**, **2**, **7**, **10**, **13**, **14**, **15**, **18**, **20** and **23**) inhibited *α*-amylase with different potencies, while the others were inactive. Compounds **13** and **15** showed $IC_{50}$ values of 73.9 ± 5.9 and 69.4 ± 3.1 μM, respectively, somewhat higher than acarbose (26.3 ± 1.2 μM) (Figure 1a). On the other hand, in the *α*-glucosidase inhibition test, a number of test compounds showed $IC_{50}$ values lower than acarbose (402.7 ± 15.5 μM), a well-known *α*-glucosidase inhibitor (Figure 1b). Among the coumarins (**1**-**3**, **7**-**11**), compounds **1**, **7**, **10**, and **11** were more active than acarbose. These data confirmed those reported in the literature for fraxetin (**11**), an inhibitor of glycolytic enzymes that control glucose metabolism in the liver and kidneys, resulting in a substantial reduction in the risk of type 2 diabetes.[7] The new eriodictyol derivative **4** showed the best activity ($IC_{50}$ 28.1 ± 2.6 μM) in the present study, and was found to be ten times more active than acarbose.

Molecular modeling studies were carried out in order to propose a possible binding mode for compound **4** inside the catalytic site of the *α*-1,4-glucosidase (EC 3.2.1.20). To date, there are no crystal structures for this target; thus, a homology modeling study was developed. The search for templates pointed to oligo-1,6-glucosidase from *Saccharomyces cerevisiae* (EC 3.2.1.10) as the enzyme endowed with the highest sequence similarity (72% of amino acid sequence identity). Both *α*-1,4-glucosidase and oligo-1,6-glucosidase belong to the retaining glycoside hydrolase (GH) family 13 for which the members share, in addition to a good amino acid sequence similarity, four highly conserved regions (I-IV) and three catalytic negative residues (two aspartate and one glutamate), that control the hydrolytic activity of the enzyme.[34] Starting from the alignment shown in Figure S26 (Supporting Information), an initial model of *α*-1,4-glucosidase was created and subjected to a simulated annealing protocol by means of the Modeller program.[35] The backbone

structure of the best-ranked model was evaluated using the Procheck software.[36] The Psi/Phi Ramachandran plot calculated for the model (Figure S27, Supporting Information) revealed that only E530 has a disallowed geometry, while two other residues (I73 and L225) showed a partially disallowed geometry. However, these residues are located outside of the binding pocket and belong to loop regions. Furthermore, as shown in Figure S28 (Supporting Information), the superimposition between the newly generated *α*-glucosidase model and the crystal structure of oligo-1,6-glucosidase highlighted that the three catalytic residues, essential for the hydrolytic activity, are conserved (D214, E276 and D349). Compound **4** was docked into the catalytic site of the *α*-1,4-glucosidase model by using a robust AUTODOCK procedure;[37] this method has already shown good in a virtual screening study on protein-protein interaction inhibitors investigated previously in our laboratory.[38] Two hundred different docking poses were generated and clustered taking as a limit value a root-mean square deviation (RMSD) of 2.0 Å. Six main clusters were obtained and evaluated for further studies. For each cluster, a representative docking pose was chosen and subjected to Molecular Docking (MD) simulation in order to assess the stability of the different supposed binding modes. The MD protocol was tested by using the X-ray complex of oligo-1,6-glucosidase with maltose (PDB code 3A4A). The complex was subjected to a total of 50 ns of MD simulation. As shown in Figure S29 (Supporting Information) after about 200 ps the system reached an equilibrium, since the total energy for the residual 49.8 ns remained approximately constant. By analyzing the RMSD of the position of the ligand with respect to the X-ray structures during the simulation, it showed an average RMSD of its heavy atoms of about 0.8 Å. The same MD protocol was then applied to the six *α*-glucosidase-**4** complexes predicted by docking calculations.

The six trajectories obtained in this way were further analyzed through the Molecular Mechanics e Poisson Bolzmann Surface Area (MM-PBSA) method[39], which has been shown to accurately estimate the ligand-receptor energy interaction.[40] This approach averages the contributions of gas phase energies, solvation free energies, and solute entropies calculated for snapshots of the complex

molecule as well as the unbound components, extracted from MD trajectories, according to the procedure fully described in the Experimental Section. The MM-PBSA results (Table 3) suggested that the fourth docking pose was the most favorable, as it showed an interaction energy ΔPBSA = -20.2 kcal/mol, more than 4 kcal/mol higher than all the other binding poses. Furthermore, the RMSD analysis of the position of the ligand with respect to the input docking pose 4 highlighted that compound **4** maintained its binding conformation and orientation in the receptor, with an average RMSD value of 0.6 Å, calculated for the heavy atoms of the ligand (Figure S30, Supporting Information). For these reasons, pose 4 was considered as the most reliable binding mode for this compound. Figure 2 shows the minimized average structure of the $\alpha$-glucosidase model complexed with compound **4** in the hypothesized binding mode (pose 4) obtained from all the 50 ns of the MD simulation. The hydroxy group at C-5 of the central chromone forms a hydrogen bond with the catalytic residues D349 and, by means of two water molecules, gives several water-bridged interactions with the second catalytic residue D214 and the other surrounding amino acids (R212, H348 and R212). Furthermore, the hydroxy group at C-5 shows an intramolecular hydrogen bond with the carbonylic oxygen at C-4 that is also connected with R312 through one water molecule. The hydroxy groups of the catechol portion form stable hydrogen bonds with D408, N412 and the backbone nitrogen of R312 and a water-mediated interaction with Y155, N412 and the backbone of F157. Finally, the aliphatic side chain of compound **4** interacts into a deep small hydrophobic cavity mainly defined by T215, L218, H245, V277 and A278.

In summary, twenty-three compounds (**1**-**23**), including six new structures (**1**-**6**), were isolated and characterized from the aerial parts of *A. thymifolium*. The new (2*S*)-7-prenyloxy-eriodictyol (**4**) exhibited high $\alpha$-glucosidase inhibitory activity with an $IC_{50}$ of 28.1 ± 2.6 μM. Modeling studies suggested that **4** binds this enzyme by interacting with the catalytic residue D349 and, by means of water molecules, it interacts also with the second catalytic residue D214 and the other surrounding amino acids.

## EXPERIMENTAL SECTION

**General Experimental Procedures.** A JASCO DIP-370 digital polarimeter with a sodium lamp (589 nm) and 1 dm microcell was used to measure optical rotations. Concentrations (*c*) are given in g/100 mL. UV spectra were registered on a Perkin-Elmer-Lambda spectrophotometer. NMR experiments were recorded on a Bruker DRX-600 spectrometer equipped with a Bruker 5 mm TCI CryoProbe and a Bruker Avance 250 spectrometer at 300 K, acquiring the spectra in methanol-$d_4$. Standard pulse sequences and phase cycling were used for TOCSY, HSQC, DQF-COSY, HMBC, and ROESY NMR experiments. NMR data were processed using XWIN-NMR software. HRESIMS were obtained in the positive- and negative-ion mode on a Q-TOF premier spectrometer equipped with a nanospray ion source (Waters Milford, MA, USA). ESIMS were obtained from an LCQ Advantage ThermoFinnigan spectrometer (ThermoFinnigan, USA). Column chromatography was performed over Sephadex LH-20 and using an Isolera® Biotage® flash purification system (silica gel 60 SNAP cartridges). HPLC analysis was performed using a Shimadzu LC-8A series pumping system equipped with a Shimadzu RID-10A refractive index detector and Shimadzu injector on a $C_{18}$ μ-Bondapak column (30 cm × 7.8 mm, 10 μm Waters, flow rate 2.0 mL $min^{-1}$). TLC separations were carried out using silica gel 60 $F_{254}$ (0.20 mm thickness) plates (Merck). GC analysis was performed using a Dani GC 1000 instrument on a L-CP-Chirasil-Val column (0.32 mm × 25 m) working with the following temperature program: 100 °C for 1 min, ramp of 5 °C/min up to 180 °C; injector and detector temperature 200 °C; carrier gas $N_2$ (2 mL/min); detector dual FID; split ratio 1:30; injection 5 μL. All spectrophotometric measurements were done in 96-well microplates on a UV/VIS spectrophotometer (SPECTROstar$^{Nano}$, BMG Labtech). Sodium phosphate, sodium chloride, potassium sodium tartrate tetrahydrate, sodium hydroxide, 3,5-dinitrosalicylic acid, starch, *α*-amylase from hog pancreas (CAS number: 9000-90-2), potassium phosphate monobasic, 4-nitrophenyl *α*-D-glucopyranoside, *α*-glucosidase from *Saccharomyces cerevisiae* (CAS number: 9001-42-7), and acarbose were acquired from Sigma–Aldrich (Milan,

Italy). Solvents such as *n*-hexane, chloroform, methanol, *n*-butanol, hydrochloric acid were purchased from VWR (Milan, Italy).

**Plant Material.** The aerial parts of *Arcytophyllum tyhymifolium* were collected in Riobamba, Chimborazo Province, Ecuador in August 2013. The plant was identified by taxonomic staff at the Herbarium of Jardin Botanico de Quito, Quito, Ecuador. A voucher specimen (no. 8144 *Arcytophyllum thymifolium*/1) was deposited at Herbarium Horti Botanici Pisani, Nuove Acquisizioni, Pisa, Italy.

**Extraction and Isolation.** The powdered dried aerial parts of *A. thymifolium* (700 g) were extracted with *n*-hexane, $CHCl_3$, and MeOH (3 × 2 L), to give 9.0 g, 18.2 g, and 52.5 g of the respective dried residue. Part of the $CHCl_3$ extract (5.0 g) was subjected to Isolera® Biotage® column chromatography (340 g silica SNAP cartridge, flow rate 100 mL/min), eluting with *n*-hexane-$CHCl_3$ (1:1), followed by $CHCl_3$ and increasing concentrations of MeOH in $CHCl_3$ (between 1% and 100%). Fractions of 27 mL were collected, analyzed by TLC, and grouped into 10 major fractions ($A_1$-$J_1$). Fraction $B_1$ yielded compound **8** (40 mg). Fractions $D_1$ (648 mg) and $F_1$ (100 mg) were purified by RP-HPLC with MeOH-$H_2O$ (5.5:4.5) as eluent to obtain compounds **7** (3.0 mg, $t_R$ 10 min), **10** (15.0 mg, $t_R$ 12 min), and **8** (5.0 mg, $t_R$ 19 min), from fraction $D_1$, and compounds **9** (2.0 mg, $t_R$ 10 min) and **10** (4.5 mg, $t_R$ 12 min), from fraction $F_1$, respectively. Fraction $G_1$ (319 mg) was subjected to RP-HPLC with MeOH-$H_2O$ (7:3) as eluent to give compound **4** (2.0 mg, $t_R$ 22 min). Fraction $H_1$ (290 mg) was chromatographed by RP-HPLC with MeOH-$H_2O$ (4.5:5.5) as eluent to give compounds **11** (4.7 mg, $t_R$ 10 min) and **1** (2.2 mg, $t_R$ 17 min). Fraction $J_1$ was purified by RP-HPLC with MeOH-$H_2O$ (2:3) as eluent to obtain compound **3** (2.0 mg, $t_R$ 23 min).

The MeOH extract (40 g) was partitioned between *n*-BuOH and $H_2O$ to give 9.5 g of a *n*-BuOH residue. Sephadex LH-20 column chromatography (5 × 100 cm) was employed to separate the *n*-BuOH soluble fraction (9.5 g), using as eluent MeOH, at flow rate of 1.5 mL/min, with fractions of 12 mL collected and grouped into twelve major fractions ($A_2$-$L_2$). Fractions $J_2$ and $L_2$ gave pure

compounds **12** (185 mg) and **13** (72.4 mg), respectively. Fraction $C_2$ (235 mg) was purified by RP-HPLC with MeOH-$H_2O$ (3:7) as eluent to yield compounds **15** (2.5 mg, $t_R$ 5 min), **16** (1.2 mg, $t_R$ 9 min), and **17** (5.4 mg, $t_R$ 34 min). Fraction $D_2$ (322 mg) was subjected to RP-HPLC with MeOH-$H_2O$ (3.5:6.5) to yield compounds **18** (3.0 mg, $t_R$ 5 min), **15** (5.0 mg, $t_R$ 6 min), **20** (14.5 mg, $t_R$ 8 min), and **17** (6.0 mg, $t_R$ 14 min). Fractions $E_2$ (314 mg), $F_2$ (127 mg), and $G_2$ (146 mg) were chromatographed over RP-HPLC with MeOH-$H_2O$ (1:2) to obtain compounds **19** (4.2 mg, $t_R$ 5 min), **20** (2.0 mg, $t_R$ 7 min), **21** (1.5 mg, $t_R$ 25 min), and **5** (1.0 mg, $t_R$ 32 min), from fraction $E_2$, compound **6** (1.2 mg, $t_R$ 16 min), from fraction $F_2$, and compounds **22** (3.0 mg, $t_R$ 13 min), **2** (1.0 mg, $t_R$ 15 min), **14** (4.9 mg, $t_R$ 24 min), and **10** (1.5 mg, $t_R$ 55 min), from fraction $G_2$, respectively. Fraction $H_2$ (238 mg) was purified by RP-HPLC with MeOH-$H_2O$ (4.5:5.5) to yield compounds **23** (10 mg, $t_R$ 6 min), **11** (5.5 mg, $t_R$ 10 min), **14** (3.4 mg, $t_R$ 13 min), and **10** (1.5 mg, $t_R$ 30 min).

*5'-Hydroxy-3'-dehydro-toddanin (**1**):* pale yellow amorphous powder; $[\alpha]_D^{25}$ -33 (*c* 0.08, MeOH); UV (MeOH) $\lambda_{max}$ (log $\varepsilon$) 253 (4.05), 270 sh (3.05), 304 (3.85), 345 (3.92) nm; $^1$H and $^{13}$C NMR, see Table 1; HRESIMS *m/z* 291.0803 $[M + H]^+$ , 313.0657 $[M + Na]^+$ (calcd for $C_{15}H_{15}O_6$ 291.0869).

*6-Demethyl-5'-hydroxy-3'-dehydro-toddanin (**2**):* pale yellow amorphous powder; $[\alpha]_D^{25}$ -40 (*c* 0.05, MeOH); UV (MeOH) $\lambda_{max}$ (log $\varepsilon$) 254 (3.95), 270 sh (3.10), 305 (3.77), 347 sh (3.88) nm; $^1$H and $^{13}$C NMR, see Table 1; ESIMS *m/z* 275 $[M - H]^-$, 245 $[M - H - 30]^-$, 201 $[M - H - 30 - 44]^-$; HRESIMS *m/z* 277.0698 $[M + H]^+$ (calcd for $C_{14}H_{13}O_6$ 277.0712).

*(2'R)-7-Hydroxy-8-(2',3'-dihydroxyisopentyl)-6-methoxycoumarin (**3**):* amorphous powder; $[\alpha]_D^{25}$ -6 (*c* 0.15, MeOH); UV (MeOH) $\lambda_{max}$ (log $\varepsilon$) 230 sh (3.66), 257 sh (3.84), 345 (4.00) nm; $^1$H and $^{13}$C NMR, see Table 1; ESIMS *m/z* 293 $[M - H]^-$, 278 $[M - H - 15]^-$, 205 $[M - H - 88]^-$, 190 $[M - H - 88 - 15]^-$; HRESIMS *m/z* 293.1046 $[M - H]^-$, 278.0853 $[M - H - 15]^-$, 205.0618 $[M - H - 88]^-$, 190.0384 $[M - H - 88 - 15]^-$ (calcd for $C_{15}H_{17}O_6$ 293.1025).

*(2S)-7-Prenyloxy-eriodictyol (**4**):* light orange amorphous powder; $[\alpha]_D^{25}$ -37(*c* 0.08, MeOH); UV (MeOH) $\lambda_{max}$ (log $\varepsilon$): 288 (4.19), 330 (3.90); CD $[\theta]_{25}$ (*c* 0.05, MeOH, nm) – 5200 (270 nm), +

5100 (326 nm); $^{1}H$ and $^{13}C$ NMR data, see Table 2; HRESIMS *m/z* 379.1166 $[M + Na]^+$ (calcd for $C_{20}H_{20}O_6Na$ 379.1158).

*10-O-p-Hydroxybenzoyl deacetyl asperulosidic acid methyl ester (**5**):* brownish amorphous powder; $[\alpha]_D^{25}$ -57 (*c* 0.1, MeOH); UV (MeOH) $\lambda_{max}$ (log $\varepsilon$) 252 (3.90), 340 sh (3.76) nm; $^{1}H$ and $^{13}C$ NMR, see Table 2; ESIMS *m/z* 523 $[M - H]^-$, 361 $[M - H - 162]^-$, 547 $[M + Na]^+$, 385 $[M + Na - 162]^+$; HRESIMS *m/z* 523.1459 $[M - H]^-$ (calcd for $C_{24}H_{27}O_{13}$ 523.1452).

*10-O-p-Hydroxybenzoyl deacetyl asperuloside (**6**):* brownish amorphous powder; $[\alpha]_D^{25}$ -79 (*c* 0.07, MeOH); UV (MeOH) $\lambda_{max}$ (log $\varepsilon$) 245 (3.93) nm; $^{1}H$ and $^{13}C$ NMR, see Table 2; ESIMS *m/z* 491 $[M - H]^-$, 329 $[M - H - 162]^-$, 515 $[M + Na]^+$, 353 $[M + Na - 162]^+$; HRESIMS *m/z* 491.4320 $[M - H]^-$ (calcd for $C_{23}H_{23}O_{12}$ 491.4217).

**Acid Hydrolysis of Compounds 5 and 6.** Acid hydrolysis of compounds **5** and **6** was carried out as reported in a previous report.[41] D-Glucose was identified as the sugar moiety in each case by comparison with retention time of an authentic sample.

***α*-Amylase and *α*-Glucosidase Enzymatic Assays.** The inhibition assay with *α*-amylase from hog pancreas was performed using the method of Saltos et al. with slight modifications.[5] Acarbose, a widely used clinical antidiabetic drug, was used as positive control. Sample solutions were prepared by dissolving each sample in 25% water-methanol at different concentrations. A substrate solution was prepared with 1% starch dissolved in 20 mM sodium phosphate buffer solution (SPBS, pH 6.9 with 6.7 mM NaCl). The enzyme (50 units/mL of *α*-amylase in SPBS, 10 µL) and sample solutions (10 µL) were mixed in Eppendorf vials, and the mixtures were incubated at 25 °C for 10 min. Then, 10 µL of substrate solution were added to each tube, and the reaction mixture was incubated at 25 °C for 10 min. The reaction was terminated by the addition of 20 µL of dinitrosalicylic acid color reagent. Subsequently, the test tubes were heated for 10 min at 100 °C. After cooling at room temperature, 300 µL of distilled water were added and the absorbance was measured at 540 nm. The absorbance of blank (enzyme solution was added during the boiling) and negative control (25% water-methanol) was recorded. Analyses were performed in triplicate and the

final sample absorbance was obtained by subtracting its corresponding blank reading. Inhibitory activity (%) was calculated as follows:

$$\%\ inhibition = \left(1 - \frac{A_{540}\ sample}{A_{540}\ negative\ control}\right) * 100$$

The $\alpha$-glucosidase inhibition assay was performed according to the procedure described by Dekdouk et al.[42] The test samples and acarbose, used as positive control, were dissolved in 25% water-methanol. Sample wells included an aliquot of 40 µL of test substances (triplicates), 130 µL of potassium phosphate buffer solution (PPBS, 10 mM, pH 7), and 60 µL of substrate (4-nitrophenyl $\alpha$-D-glucopyranoside 2.5 mM) dissolved in PPBS. Absorbance was measured at 405 nm ($T_{0'}$), then the reaction was initiated by the addition of 20 µL of enzyme stock solution (0.28 units/mL in PPBS). Plates were incubated at 37 °C for 10 min and, after incubation, the absorbance was measured again ($T_{10'}$). For the negative control wells, the samples were substituted with 40 µL of 25% water-methanol. The inhibition percentage was calculated according to the following equation:

$$\%\ inhibition = \left(1 - \frac{A_{405}\ sample_{(T_{10'} - T_{0'})}}{A_{405}\ negative\ control_{(T_{10'} - T_{0'})}}\right) * 100$$

Each concentration of sample required to inhibit the activity of an enzyme by 50% ($IC_{50}$) was derived from three independent experiments. $IC_{50}$ values were determined by using GraphPad Prism 5 Software (San Diego, CA, USA) and they were estimated by nonlinear curve-fitting and presented as their respective 95% confidence limits. Data are expressed as the means ± standard error (SD) of three independent experiments. They were considered statistically significant with $p$ values of $<0.05$.

**Homology Modeling.** The primary sequence of $\alpha$-1,4-glucosidase was acquired from the SWISS-PROT protein sequence database (code P53341).[43] The search for sequence similarity was carried out employing pBlast[44] and the crystal structure of oligo-1,6-glucosidase was obtained from the Protein Data Bank[45] (PDB code 3A4A). Therefore, the sequence alignment was performed by means of CLUSTAL W software,[46] with a gap open penalty of 10 and a gap extension penalty of 0.05. Starting from the resulting alignment, five structures were generated through the "very slow MD annealing" refinement method of the Modeller program. Taking into account the DOPE (discrete optimized protein energy) values, the best enzyme model was chosen. The backbone conformation of the so obtained enzyme structure was then evaluated by the analysis of the Psi/Phi Ramachandran plot acquired using PROCHECK.

**Molecular Modeling Studies of Compound 4.** Compound **4** was built using Maestro and was then energy-minimized employing a water environment model (generalized-Born/surface-area model) by means of Macromodel.[47] The minimization was performed using the conjugated gradient method, the MMFFs force field and a distance-dependent dielectric constant of 1.0, until a convergence value of 0.05 kcal/(Å·mol) was achieved. The ligand was docked into the catalytic pocket of the $\alpha$-1,4-glucosidase model by means of AUTODOCK4.2.[37] The docking site used for calculation was defined superimposing the enzyme model obtained to the template structure (PDB code 3A4A) and setting bound maltose as the center of a grid of 56 points, respectively, in the x, y, and z directions. The energetic map calculation was carried out by using a grid spacing of 0.375 Å and a constant distance-dependent function of the dielectric. Compound **4** was subjected to 200 runs of an AUTODOCK calculation employing a robust procedure with 10,000,000 steps of energy evaluation; the number of individuals in the initial population was set to 500 and a maximum of 10,000,000 generations was simulated in each docking run. An rms tolerance of 2.0 Å was applied in order to cluster the docking solutions and all the other settings were set as default. The six clusters of poses with a population higher than 10% among all the generated docking solutions were considered for further studies.

**Molecular Dynamics Simulations.** All simulations were performed by means of AMBER14.[48] The simulation procedure was set up using as reference structure the X-ray complex of oligo-1,6-glucosidase with maltose (PDB code 3A4A).[49] The six different ligand-protein complexes obtained from the docking calculation were placed in a cubic water-box and solvated with a 20 Å water cap; an explicit solvent model for water was used (TIP3P). Sodium ions were added as counter ions in order to neutralize the system. The General Amber Force Field (GAFF) parameters were appointed to compound **4**, whereas the partial charges were calculated using the AM1-BCC as implemented in the Antechamber suite. Before running MD simulations, the complex was energy-minimized by means of 1,000 steps of steepest descent followed by 2,000 steps of conjugate gradient, for a total of 3,000 steps of energy minimization, until a convergence of 0.05 kcal/(mol·Å) was reached. A position restraint of 10.0 kcal/(mol·Å) was applied to the protein $\alpha$ carbons in order to clamp the protein backbone. MD trajectories were run employing the thus obtained minimized complexes as starting conformations; particle mesh Ewald (PME) electrostatics and periodic boundary conditions were used in the simulations.[50] Three different steps of MD simulations were run employing a cut-off of 10 Å for the non-bonded interaction and SHAKE algorithm to keep rigid every bond involving hydrogen. In the first step, a 0.5 ns of constant-volume simulation was carried out to increase the temperature from 0 to 300 K. The second MD step consisted of 49.5 ns of constant-pressure simulation, in which the temperature was maintained constant at 300 K by using the Langevin thermostat. In both these two steps, a harmonic force of 10 kcal/(mol·Å) was applied to block the protein $\alpha$ carbon, as in the minimization stage.

**Binding Energy Evaluation.** The binding energy associated with the different six ligand-protein complexes analysed through MD simulations was evaluated by means of AMBER 14. Starting from the total 50 ns of the MD trajectories of each ligand-protein complex, 500 snapshots were extracted and used for the calculation (at a time interval of 10 ps). The average total energy (G) for the analysed macromolecular systems was computed adding the various MM-PBSA energy terms explained in the following equation:

$$G = Gpolar + Gnonpolar + Emm - TS$$

Polar energies (Gpolar) were calculated using the Poisson-Boltzmann and Generalized Born methods with the MM-PBSA module of AMBER 14, applying dielectric constants of 1 and 80 to embody the gas and the water phases, respectively. Non-polar energies (Gnonpolar) were obtained employing the MOLSURF program; while electrostatic, van der Waals and internal energies (Emm) were determined by means of the SANDER module of AMBER 14. The entropic value (TS) was considered as approximately constant in the comparison between the energetic interactions of the ligand and the protein.

## ASSOCIATED CONTENT

**Supporting Information.** HRESIMS and NMR spectra of compounds **1**-**6**; sequence alignment; Ramachandran plot; binding site analysis; MD simulations analysis. This material is available via the Internet at http://pubs.acs.org.

## AUTHOR INFORMATION


### Corresponding Author

* Tel: +39-089-969754. Fax: +39-089-969602. E-mail: detommasi@unisa.it.


### Notes

The authors declare no competing financial interest.

**REFERENCES**


(1) Mena, V. P. *Mem. New York Bot. Gard*. **1990**, 60, 1-26.

(2) Sklenář, P.; Balslev, H. *Flora* **2007**, *202*, 50-61.

(3) Monigatti, M.; Bussmann, R. W.; Weckerle, C. S. *J. Ethnopharmacol.* **2013**, *145*, 450-464.

(4) De Feo, V.; della Valle, C.; De Simone, F.; Pizza, C. *Ann. Chim.* **1992**, *82*, 476-486.

(5) Saltos, M. B. V.; Puente, B. F. N.; Faraone, I.; Milella, L.; De Tommasi, N.; Braca, A. *Phytochemistry Lett.* **2015**, *14*, 45-50.

(6) Saltos, M. B. V.; Puente, B. F. N.; Milella, L.; De Tommasi, N.; Dal Piaz, F.; Braca, A. *Planta Med.* **2015**, *81*, 1056-64.

(7) Murali, R.; Srinivasan, S.; Ashokkumar, N. *Biochimie* **2013**, *95*, 1848-1854.

(8) Cao, H.; Chen, X. *Anticancer Agents Med. Chem.* **2012**, *12*, 929-939.

(9) Manaharan, T.; Teng, L. L.; Appleton, D.; Ming, C. H.; Masilamani, T.; Palanisamy, U. D. *Food Chem.* **2011**, *129*, 1355-1361.

(10) Kim, K. E.; Ko, K. H.; Heo, R. W.; Yi, C..; Shin, H. J.; Kim, J. Y.; Park, J. H.; Nam, S.; Kim, H.; Roh, G. S. *J. Med.* **2016**, *19*, 290-9.

(11) Miura, T.; Nishiyama, Y.; Ichimaru, M.; Moriyasu, M.; Kato, A. *Biol. Pharm. Bull.* **1996**, *19*, 160-161.

(12) Giang, V. H.; Ban, N. K.; Nhiem, N. X.; Kiem, P.; Minh, C.; Anh, H. L. T.; Yen, P. H.; Tai, B. H.; Cuong, N. X.; Nam, N. H. *Bull. Kor. Chem. Soc.* **2013**, *34*, 1555-1558.

(13) McCarty, M. F. *Med. Hypotheses* **2005**, *64*, 848-853.

(14) Wardrop, D. J.; Waidyarachchi, S. L. *Nat. Prod. Rep.* **2010**, *27*, 1431-1468.

(15) Sels, J. P. J. E.; Huijberts, M. S. P.; Wolffenbuttel, B. H. R. *Expert Opin. Pharmacother*. **1999**, *1*, 149-156.

(16) Teng, H.; Chen, L. *Crit. Rev. Food Sci. Nutr.* **2016**, (*Epub 2016 Feb 6* just-accepted).

(17) Amaro-Luis, J. M.; Massanet, G. M.; Pando, E.; Rodriguez-Luis, F.; Zubia, E. *Planta Med.* **1990**, *56*, 304-306.

(18) Tsai, I. L.; Wun, M. F.; Teng, C. M.; Ishikawa, T.; Chen, I. S. *Phytochemistry* **1998**, *48*, 1377-1382.

(19) Di Bari, L.; Pescitelli, G.; Pratelli, C.; Pini, D.; Salvadori, P. *J. Org. Chem.* **2001**, *66*, 4819-4825.

(20) Garo, E.; Wolfender, J. L.; Hostettmann, K.; Hiller, W.; Antus, S.; Mavi, S. *Helv. Chim. Acta* **1998**, *81*, 754-763.

(21) Slade, D.; Ferreira, D.; Marais, J. P. *Phytochemistry* **2005**, *66*, 2177-2215.

(22) Otsuka, H.; Yoshimura, K.; Yamasaki, K.; Cantoria, M. C. *Chem. Pharm. Bull.* **1991**, *39*, 2049-2052.

(23) Mondon, A.; Callsen, H. *Chem. Ber.* **1975**, *108*, 2005-2020.

(24) Chen, Y. H.; Chang, F. R.; Wu, C. C.; Yen, M. H.; Liaw, C. C.; Huang, H. C.; Kuo, Y. H.; Wu, Y. C. *Planta Med.* **2006**, *72*, 75.

(25) Okuyama, E.; Okamoto, Y.; Yamazaki, M.; Satake, M. *Chem. Pharm. Bull.* **1996**, *44*, 333-336.

(26) De Almeida, A.; Miranda, M.; Simoni, I.; Wigg, M.; Lagrota, M.; Costa, S. *Phytother. Res.* **1998**, *12*, 562-567.

(27) Agrawal, P. K. *Carbon-13 NMR of Flavonoids;* Elsevier: Amsterdam, **1989**, p 13.

(28) Han, Y.; Nishibe, S.; Noguchi, Y.; Jin, Z. *Phytochemistry* **2001**, *58*, 577-580.

(29) Demirezer, L. Ö.; Gürbüz, F.; Güvenalp, Z.; Ströch, K.; Zeeck, A. *Turk. J. Chem.* **2006**, *30*, 525-534.

(30) Kim, D.-H.; Lee, H.-J.; Oh, Y.-H.; Kim, M.-J.; Kim, S.-H.; Jeong, T.-S.; Baek, N.-I. *Arch. Pharm. Res*. **2005**, *28*, 1156-1160.

(31) Chaudhuri, R. K.; Afifi-Yazar, F. U.; Sticher, O. *Tetrahedron* **1980**, *36*, 2317-2326.

(32) Zhu, X.; Dong, X.; Wang, Y.; Ju, P.; Luo, S. *Helv. Chim. Acta* **2005**, *88*, 339-342.

(33) Iwai, K.; Kishimoto, N.; Kakino, Y.; Mochida, K.; Fujita, T. *J. Agric. Food Chem.* **2004**, *52*, 4893-4898.

(34) Yamamoto, K.; Miyake, H.; Kusunoki, M.; Osaki, S. *FEBS J.* **2010**, *277*, 4205-4214.

(35) Fiser, A.; Do, R. K.; Sali, A. *Protein Sci.* **2000**, *9*, 1753-1773.

(36) Laskowski, R. A.; Macarthur, M. W.; Moss, D. S.; Thornton, J. M. *J. Appl. Crystallogr.* **1993**, *26*, 283-291.

(37) Morris, G. M.; Huey, R.; Lindstrom, W.; Sanner, M. F.; Belew, R. K.; Goodsell, D. S.; Olson, A. J. *J. Comput. Chem.* **2009**, *30*, 2785-2791.

(38) Poli, G.; Gelain, A.; Porta, F.; Asai, A.; Martinelli, A.; Tuccinardi, T. *J. Enzym. Inhib. Med. Ch.* **2015**, 1-7.

(39) Kollman, P. A.; Massova, I.; Reyes, C.; Kuhn, B.; Huo, S.; Chong, L.; Lee, M.; Lee, T.; Duan, Y.; Wang, W.; Donini, O.; Cieplak, P.; Srinivasan, J.; Case, D. A.; Cheatham, T. E., 3rd. *Acc. Chem. Res.* **2000**, *33*, 889-897.

(40) Tuccinardi, T.; Manetti, F.; Schenone, S.; Martinelli, A.; Botta, M. *J. Chem. Inf. Model.* **2007**, *47*, 644-655.

(41) Dal Piaz, F.; Vassallo, A.; Temraz, A.; Cotugno, R.; Belisario, M. A.; Bifulco, G.; Chini, M. G.; Pisano, C.; De Tommasi, N.; Braca, A. *J. Med. Chem.* **2013**, *56*, 1583-1595.

(42) Dekdouk, N.; Malafronte, N.; Russo, D.; Faraone, I.; De Tommasi, N.; Ameddah, S.; Severino, L.; Milella, L. *Evid.-Based Complement. Alternat. Med.* **2015**, 684925.

(43) Gasteiger, E.; Gattiker, A.; Hoogland, C.; Ivanyi, I.; Appel, R. D.; Bairoch, A. *Nucleic Acids Res.* **2003**, *31*, 3784-3788.

(44) Altschul, S. F.; Madden, T. L.; Schaffer, A. A.; Zhang, J.; Zhang, Z.; Miller, W.; Lipman, D. J. *Nucleic Acids Res.* **1997**, *25*, 3389-3402.

(45) Berman, H. M.; Westbrook, J.; Feng, Z.; Gilliland, G.; Bhat, T. N.; Weissig, H.; Shindyalov, I. N.; Bourne, P. E. *Nucleic Acids Res.* **2000**, *28*, 235-242.

(46) Thompson, J. D.; Higgins, D. G.; Gibson, T. J. *Nucleic Acids Res.* **1994**, *22*, 4673-4680.

(47) *Macromodel*, version 9.7. Schrödinger, Inc: Portland, OR, 2009.

(48) Case, D. A.; Berryman, J. T.; Betz, R. M.; Cerutti, D. S.; III, T. E. C.; Darden, T. A.; Duke, R. E.; Giese, T. J.; Gohlke, H.; Goetz, A. W.; Homeyer, N.; Izadi, S.; Janowski, P.; Kaus, J.; Kovalenko, A.; Lee, T. S.; LeGrand, S.; Li, P.; Luchko, T.; Luo, R.; Madej, B.; Merz, K. M.; Monard, G.; Needham, P.; Nguyen, H.; Nguyen, H. T.; Omelyan, I.; Onufriev, A.; Roe, D. R.; Roitberg, A.; Salomon-Ferrer, R.; Simmerling, C. L.; Smith, W.; Swails, J.; Walker, R. C.; Wang, J.; Wolf, R. M.; Wu, X.; York, D. M.; Kollman, P. A. *AMBER*, version 14. In University of California: San Francisco, CA, 2015.

(49) Yamamoto, K.; Miyake, H.; Kusunoki, M.; Osaki, S. *FEBS J.* **2010**, *277*, 4205-4214.

(50) York, D. M.; Darden, T. A.; Pedersen, L. G. *J. Chem. Phys.* **1993**, *99*, 8345-8348.

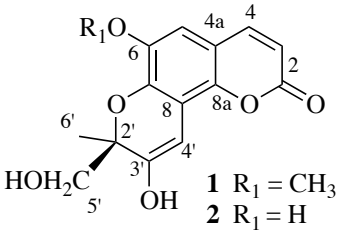

**1** $R_1 = CH_3$
**2** $R_1 = H$

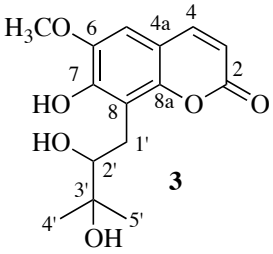

**3**

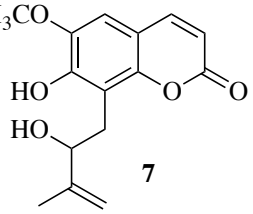

**7**

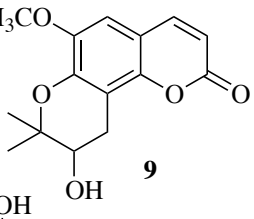

**9**

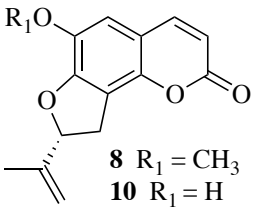

**8** $R_1 = CH_3$
**10** $R_1 = H$

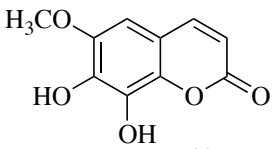

**11**

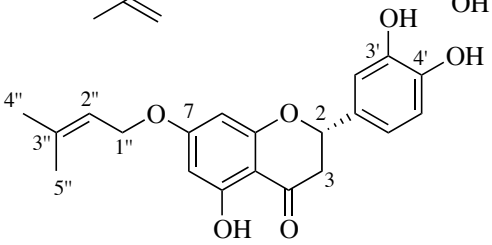

**4**

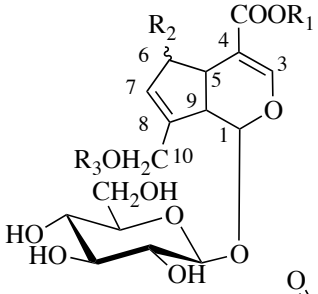

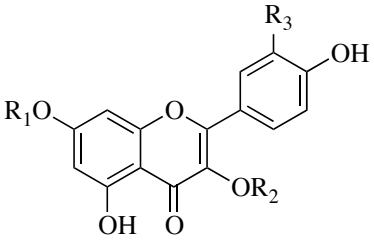

**5** $R_1 = CH_3$ $R_2 =$  $R_3 =$ 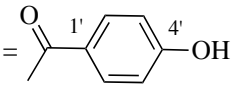

**15** $R_1 = H$ $R_2 =$  $R_3 = COCH_3$

**16** $R_1 = CH_3$ $R_2 =$  $R_3 = H$

**17** $R_1 = CH_3$ $R_2 =$  $R_3 = COCH_3$

**18** $R_1 = R_3 = H$ $R_2 =$ 

**21** $R_1 = CH_3$ $R_2 =$  $R_3 =$ 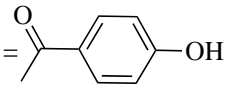

**12** $R_1 = H$ $R_2 =$ 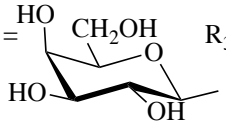 $R_3 = OH$

**13** $R_1 = CH_3$ $R_2 = H$ $R_3 = OH$

**14** $R_1 = R_3 = H$ $R_2 =$ 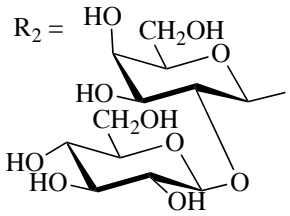

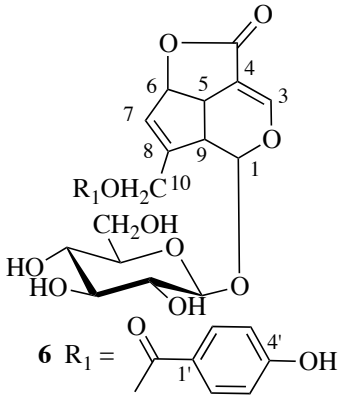

**6** $R_1 =$ 

**19** $R_1 = H$

**20** $R_1 = COCH_3$

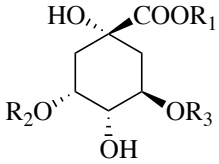

**22** $R_1 = CH_3$ $R_2 =$ 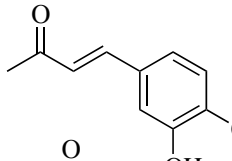 $R_3 = H$

**23** $R_1 = R_2 = H$ $R_3 =$ 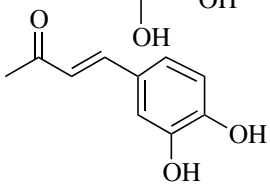

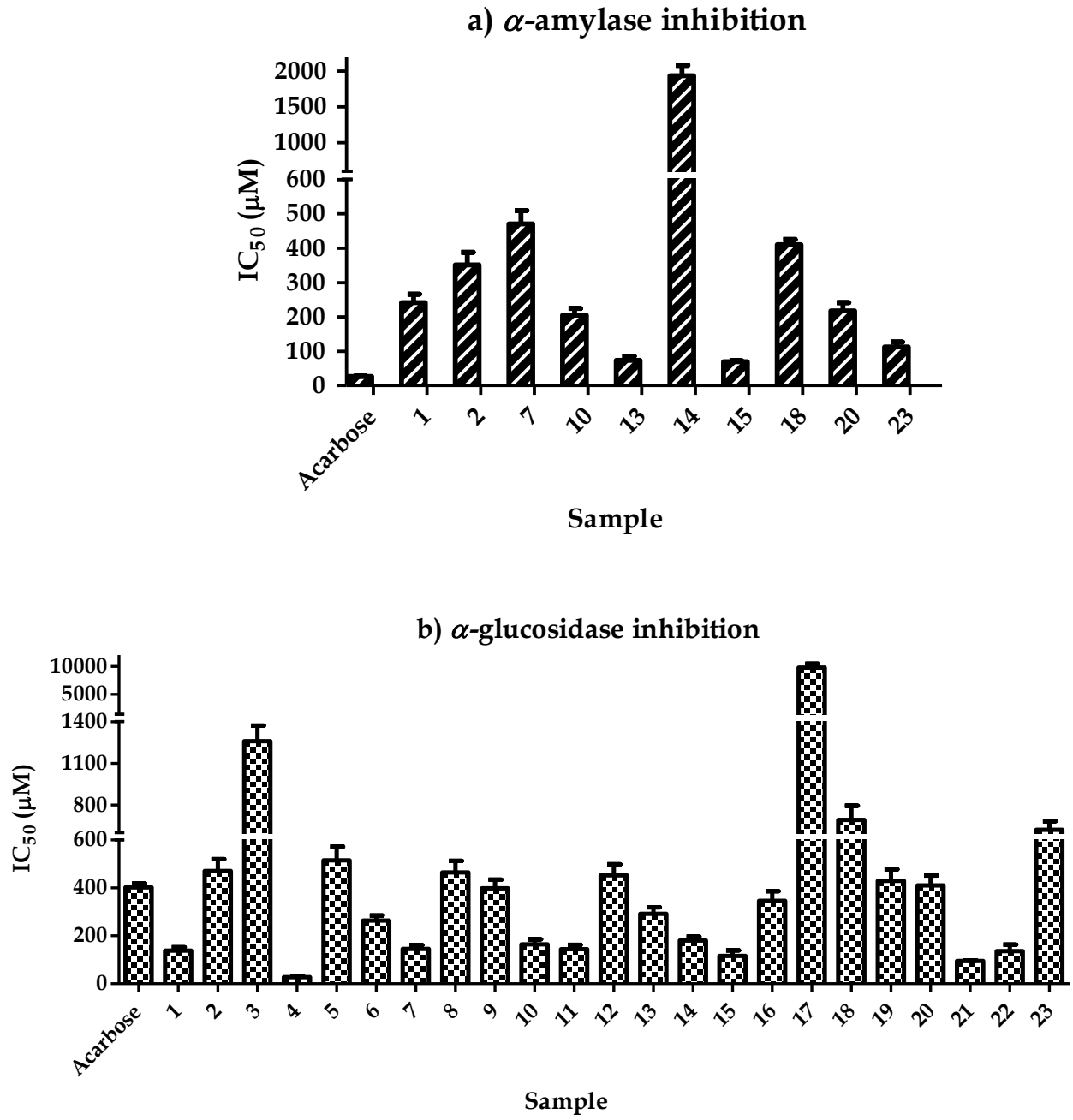


**Figure 1.** (a) *α*-Amylase and (b) *α*-glucosidase inhibition ($IC_{50}$ values in μM, data are means ± SD from three experiments) by acarbose and the isolated compounds (**1**-**23**).

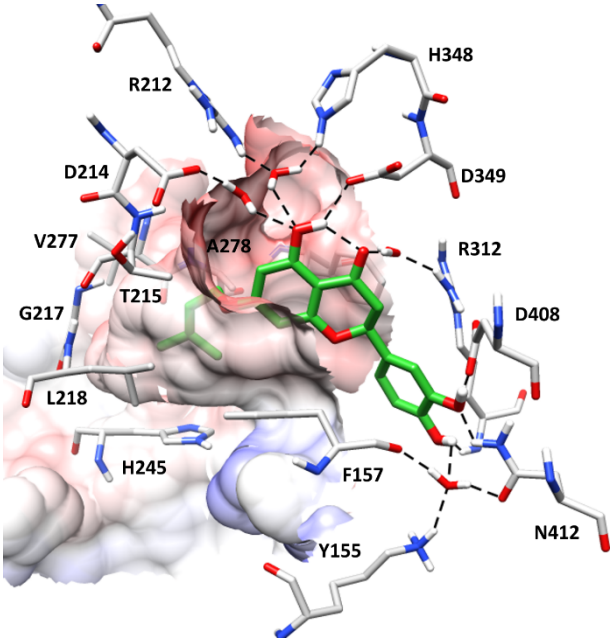


**Figure 2.** Minimized average structure of compound **4** bound to $\alpha$-1,4-glucosidase. The deep small hydrophobic cavity mainly defined by T215, G217, L218, H245, V277 and A278 is shown; the most lipophilic regions are colored red whereas the polar ones are colored blue.

**Table 1. $^{1}H$ and $^{13}C$ NMR Spectroscopic Data of Compounds 1-3 and 7[a]**

| | 1 | | 2 | | 3 | | 7 | |
|---|---|---|---|---|---|---|---|---|
| position | $\delta_H$ | $\delta_C$ | $\delta_H$ | $\delta_C$ | $\delta_H$ | $\delta_C$ | $\delta_H$ | $\delta_C$ |
| 2 | | 162.3 | | 162.5 | | 164.5 | | 164.3 |
| 3 | 6.39 d (9.4) | 114.0 | 6.39 d (9.5) | 114.3 | 6.19 d (9.5) | 111.0 | 6.21 d (9.5) | 111.5 |
| 4 | 8.06 d (9.4) | 146.8 | 7.98 d (9.5) | 146.4 | 7.88 d (9.5) | 146.6 | 7.88 d (9.5) | 146.7 |
| 4a | | 115.3 | | 115.7 | | 115.0 | | 115.0 |
| 5 | 7.06 s | 100.0 | 7.11 s | 99.5 | 7.04 s | 108.0 | 7.06 s | 108.2 |
| 6 | | 144.5 | | 143.0 | | 146.5 | | 146.5 |
| 7 | | 147.6 | | 147.0 | | 148.0 | | 148.0 |
| 8 | | 120.9 | | 120.5 | | 116.0 | | 114.5 |
| 8a | | 143.9 | | 143.7 | | 150.0 | | 149.8 |
| 1'a | | | | | 3.20 dd (13.0, 10.5) | 28.6 | 3.21dd (12.5, 10.5) | 30.4 |
| 1'b | | | | | 3.04 br d (13.0) | | 3.12 br d (12.5) | |
| 2' | | 73.0 | | 73.2 | 3.73 m | 79.4 | 4.49 m | 76.0 |
| 3' | | 164.5 | | 164.7 | | 74.0 | | 149.2 |
| 4' | 7.02 s | 105.2 | 6.97 s | 105.0 | 1.30 s | 25.0 | 4.69 m | 111.2 |
| 5' | 3.78 s | 69.0 | 3.84 s | 69.3 | 1.30 s | 24.0 | 1.87 s | 18.0 |
| 6' | 1.62 s | 24.0 | 1.65 s | 23.4 | | | | |
| $OCH_3$-6 | 4.03 s | 56.0 | | | 3.92 s | 56.3 | 3.92 s | 57.0 |

[a]Spectra were run in methanol-$d_4$ at 600 MHz ($^{1}H$) and 150 MHz ($^{13}C$). *J* values are in parentheses and reported in Hz; chemical shifts are given in ppm; assignments were confirmed by COSY, HSQC, and HMBC experiments.

**Table 2.$^{1}$H and $^{13}$C NMR Spectroscopic Data of Compounds 4-6**

| | **4**[a] | | **5**[a] | | **6**[b] | |
|---|---|---|---|---|---|---|
| position | $\delta_H$ | $\delta_C$ | $\delta_H$ | $\delta_C$ | $\delta_H$ | $\delta_C$ |
| 1 | | | 5.15 d (8.5) | 101.6 | 6.05 d (8.0) | 93.2 |
| 2 | 5.33 dd (12.0, 3.0) | 80.8 | | | | |
| 3a | 3.13 dd (17.0, 12.0) | 44.0 | 7.68 s | 155.0 | 7.32 s | 150.0 |
| 3b | 2.74 dd (17.0, 3.0) | | | | | |
| 4 | | 197.9 | | 108.0 | | 108.0 |
| 5 | | 164.8 | 3.11 br t (9.0, 2.0) | 42.0 | 3.71 br t (9.0) | 37.8 |
| 6 | 6.04 d (2.0) | 96.2 | 4.90[c] | 75.0 | 5.59 br d (1.5) | 86.0 |
| 7 | | 168.4 | 6.09 d (2.0) | 131.3 | 5.81 br s | 128.9 |
| 8 | 6.06 d (2.0) | 95.5 | | 146.0 | | 146.0 |
| 9 | | 165.0 | 2.72 br t (8.0) | 46.1 | 3.33[c] | 45.5 |
| 10a | | 104.2 | 5.25 br d (15.0) | 63.0 | 4.82 d (15.0) | 62.8 |
| 10b | | | 5.00 br d (15.0) | | 4.70 d (15.0) | |
| 11 | | | | 170.0 | | 172.3 |
| COOMe | | | 3.78 s | 51.5 | | |
| 1' | | 132.0 | | 122.0 | | 122.2 |
| 2' | 6.95 d (2.0) | 114.7 | 7.97 d (8.5) | 132.5 | 7.92 d (8.5) | 132.8 |
| 3' | | 146.8 | 6.88 d (8.5) | 116.0 | 6.86 d (8.5) | 116.0 |
| 4' | | 147.0 | | 164.0 | | 164.0 |
| 5' | 6.81[c] | 116.1 | 6.88 d (8.5) | 116.0 | 6.86 d (8.5) | 116.0 |
| 6' | 6.82[c] | 119.3 | 7.97 d (8.5) | 132.5 | 7.92 d (8.5) | 132.8 |
| CO | | | | 167.5 | | 167.8 |
| 1" | 4.58 d (7.0) | 66.5 | | | | |
| 2" | 5.44 t (6.5) | 120.0 | | | | |
| 3" | | 139.7 | | | | |
| 4" | 1.80 s | 26.0 | | | | |
| 5" | 1.76 s | 18.3 | | | | |
| Glc 1 | | | 4.77 d (7.5) | 100.1 | 4.67 d (7.8) | 99.9 |
| 2 | | | 3.25 dd (9.0, 7.5) | 74.4 | 3.21 dd (9.5, 7.8) | 74.4 |
| 3 | | | 3.38 t (9.0) | 77.9 | 3.37 t (9.5) | 77.7 |
| 4 | | | 3.29 t (9.0) | 71.2 | 3.33 t (9.5) | 71.4 |
| 5 | | | 3.33 m | 78.3 | 3.29 m | 78.1 |
| 6a | | | 3.90 dd (12.0, 3.0) | 62.6 | 3.86 dd (12.0, 2.5) | 62.4 |
| 6b | | | 3.68 dd (12.0, 4.5) | | 3.63 dd (12.0, 4.5) | |

[a]Spectra were run in methanol-$d_4$ at 600 MHz ($^{1}$H) and 150 MHz ($^{13}$C). *J* values are in parentheses and reported in Hz; chemical shifts are given in ppm; assignments were confirmed by COSY, HSQC, and HMBC experiments.
[b]Spectra were run in methanol-$d_4$ at 250 MHz.
[c]Overlapped signal.

**Table 3. MM-GBSA and MM-PBSA resulting values for the six different *α*-1,4-glucosidase-compound 4 complexes are reported[a,b]**

| | MM-PBSA Evaluation | | | | |
|---|---|---|---|---|---|
| | VDW | EEL | ESURF | EGB | ΔPBSA |
| pose 1 | -36.6 | -51.4 | 75.9 | -4.5 | -15.7 |
| pose 2 | -39.7 | -43.5 | 73.2 | -4.5 | -14.5 |
| pose 3 | -44.0 | -16.0 | 52.1 | -4.6 | -12.6 |
| pose 4 | -48.2 | -26.1 | 58.3 | -4.2 | -20.2 |
| pose 5 | -46.6 | -34.3 | 71.2 | -4.5 | -14.3 |
| pose 6 | -45.6 | -32.0 | 74.7 | -4.5 | -7.4 |

[a]ΔGBSA and ΔPBSA are the total amount of the electrostatic (EEL), van der Waals (VDW), polar (EGP/EPB) and non-polar (ESURF/ENPOLAR) solvation free energy.
[b]Data are expressed as kcal/mol.